

# Deep Video Coding with Dual-Path Generative Adversarial Network

Tiesong Zhao  
Fuzhou University  
t.zhao@fzu.edu.cn

Weize Feng  
Fuzhou University  
201127019@fzu.edu.cn

Hongji Zeng  
Fuzhou University  
201120063@fzu.edu.cn

Yuzhen Niu  
Fuzhou University  
yuzhenniu@gmail.com

Jiaying Liu  
Peking University  
liujiaying@pku.edu.cn

## Abstract

The deep-learning-based video coding has attracted substantial attention for its great potential to squeeze out the spatial-temporal redundancies of video sequences. This paper proposes an efficient codec namely dual-path generative adversarial network-based video codec (DGVC). First, we propose a dual-path enhancement with generative adversarial network (DPEG) to reconstruct the compressed video details. The DPEG consists of an  $\alpha$ -path of auto-encoder and convolutional long short-term memory (ConvLSTM), which facilitates the structure feature reconstruction with a large receptive field and multi-frame references, and a  $\beta$ -path of residual attention blocks, which facilitates the reconstruction of local texture features. Both paths are fused and co-trained by a generative-adversarial process. Second, we reuse the DPEG network in both motion compensation and quality enhancement modules, which are further combined with motion estimation and entropy coding modules in our DGVC framework. Third, we employ a joint training of deep video compression and enhancement to further improve the rate-distortion (RD) performance. Compared with x265 LDP very fast mode, our DGVC reduces the average bit-per-pixel (bpp) by 39.39%/54.92% at the same PSNR/MS-SSIM, which outperforms the state-of-the-art deep video codecs by a considerable margin.

## 1. Introduction

High efficient video compression has been a challenging task in multimedia community since 1980s. During the past four decades, the researchers have devoted to improve the rate-distortion (RD) efficiency by introducing more coding tools, such as hierarchical predictions, coding tree units and asymmetric partitions, to the hybrid video coding structure.



Figure 1. Reconstructed frames with the H.265 (x265 LDP very fast) and our DGVC. The DGVC reduces the bit-per-pixel (bpp) of H.265 by almost half whilst retaining competitive PSNR or MS-SSIM.

In each generation of video codec, these consisting efforts approximately halves the compressed bits at the same visual quality. Among them, the popular H.265/HEVC [37] and H.266/VVC [6] are considered as the newest achievements of Joint Collaborative Team on Video Coding (JCT-VC). With the widespread use of high definition (HD) videos, it is undoubtable that the video coding problem is still a critical issue in the 5G era.

The popular video codecs treat the videos as *signals*. They remove the spatial-temporal redundancies of videos by low-level transform, quantization and entropy coding. However, in computer vision community, the videos can be processed as stacked *features*, which allows us to develop end-to-end video codecs with big data and learning. Recently, the learning-based image codecs [7–10, 12, 16, 19, 21, 28, 42] have surpassed the traditional image codecs in terms of compression efficiency, which also inspires learning-based codecs for videos. In fact, we have witnessed a booming of learning-based video codecs in the past 2 years.

The learning-based video codecs utilize the deep neural networks to imitate the motion estimation (ME), mo-

tion compensation (MC), residual compression and video reconstruction [2, 14, 17, 18, 20, 23–27, 32, 33, 43, 44]. Owing the advantage of deep learning on large-scale dataset, these methods adopt convolutional neural networks (CNNs), auto-encoders, and/or generative adversarial networks (GANs) to achieve the end-to-end video compression. Among them, [43, 44] utilized bi-directional prediction while the other method utilize one-way prediction with 1 to 4 references. A separate quality enhancement network was deployed in post-processing stage of [43]. Early works exhibited superior performances than H.264/AVC or competitive performances compared with H.265/HEVC [2, 14, 26, 33]. Recently, the deep video codecs have surpassed the H.265/HEVC in terms of RD performance [17, 18, 20, 23–25, 27, 32, 43, 44].

Despite of these great efforts, the RD performance of deep video coding is still inferior to the newest reigning video codec, H.266/VVC. It is imperative to further improve the RD efficiency with deep networks. In this paper, we move the next step to propose an efficient deep video codec that benefits from GAN-based visual enhancement. The conventional GAN generates visually pleasing results by no-reference evaluation and is not well capable of precise reconstruction of original frames. To improve the full-reference reconstruction quality, we introduce the residual attention blocks (RABs) as a parallel path. This dual-path GAN is co-trained by a generative-adversarial process to well reconstruct the video frames after quantization, where a convolutional long short-term memory (ConvLSTM) network [35] is also introduced to refer to multiple coded frames. In our codec, this design is reused in both MC and perceptual enhancement while the optical flow, auto-encoders and residual networks are utilized to construct the other modules. Aimed at an optimal RD performance, we employ a joint training of deep video compression and enhancement. Figure 1 depicts the superior RD performances of our method compared with H.265.

Our main contributions are summarized as follows.

**A dual-path enhancement with GAN (DPEG) for video reconstruction:** We propose the DPEG with two paths of different receptive fields. An  $\alpha$ -path focuses on the structure features with auto-encoder and ConvLSTM. A  $\beta$ -path focuses on the texture details with RABs. The fusion of these features improves the visual quality of video frames and also reduces the bpp for residual coding.

**A DPEG-based deep video codec (DGVC):** We propose the DGVC framework by reusing DPEG network in both MC and perceptual enhancement. The other modules of our DGVC are constructed by CNN-based optical flow, auto-encoder and residual networks.

**Joint training of video compression and enhancement:** We employ a joint training of compression and enhancement in DGVC framework, in order to achieve an op-

timal tradeoff between compressed bits and reconstructed quality. Experimental results reveal the effectiveness of our DGVC with joint training.

## 2. Related Work

**Deep image compression.** The reigning image codecs, such as JPEG [39], JPEG2000 [38] and BPG [3], employ the frequency transform and quantization to remove the spatial redundancies of images. While in deep image codecs, the auto-encoders, recurrent neural networks (RNNs) and GANs are widely used. Recent efforts have supported spatial rate allocation, *i.e.*, to allocate bits based on the spatial textures and contexts [7, 10, 12, 19, 21] or multiple bpps with one network [8, 42]. In [9], a CNN-based ProxIQa model was proposed to mimic the perceptual model for RD tradeoff. In [12], the discretized Gaussian mixture likelihoods were utilized to parameterize the latent code distributions, aimed at a more accurate and flexible entropy model. In [16], a checkerboard context model was proposed to support parallel image decoding. In [28], the CNN was employed to design a wavelet-like transform for removing redundancies. These methods exploits the spatial correlations of single pictures, while our DGVC framework focuses on the spatial-temporal correlations of successive pictures, especially the MC module based on DPEG.

**Deep video compression.** By removing the spatial-temporal redundancies of videos, the reigning video codecs, such as H.265/HEVC and H.266/VVC, achieve significantly higher compression efficiency than those image codecs. These characteristics have also been utilized in deep video coding. A classic method, called deep video compression (DVC) [26], replicated the ME/MC, transform/quantization and entropy coding with optical flow, non-linear residual encoder and CNN, respectively. In [25], an error-propagation-aware training was proposed to address the error propagation and content adaptive compression in DVC. In [27], two variants of DVC, DVC Lite and DVC Pro, were designed with different coding complexities. In [23], the CNN-based motion vector (MV) prediction, MV refinement, multi-frame MC and residual refinement were introduced to develop the multiple frames prediction for learned video compression (M-LVC). In [43], the hierarchical learned video compression (HLVC) introduced the hierarchical group-of-picture (GOP) structure which had shown its high efficiency since H.264 scalable coding. It also utilized a weighted recurrent quality enhancement to further improve the visual quality at decoder-end. In [44], a recurrent learned video compression (RLVC) employed the recurrent auto-encoder and recurrent probability model for improved MV and residual compression.

The rate allocation of deep video coding was first realized by [14] and [33], which utilized the deep generative model and recursive network for high compression effi-

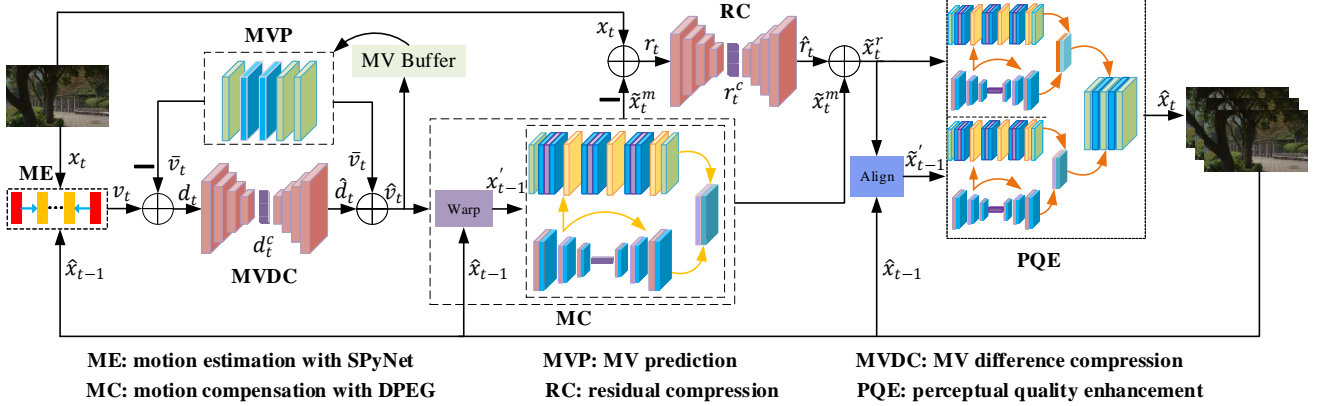


Figure 2. The framework of our DGVC encoder, where the proposed DPEG network is utilized in both MC and PQE modules. For a frame  $x_t$ , the ME module calculates its MV  $v_t$  with SPyNet and bi-directional IPPP structure. Meanwhile, the MVP module derives an MV prediction,  $\bar{v}_t$ , based on an MV buffer of references. The MVDC module compresses and reconstructs the MV difference  $d_t = v_t - \bar{v}_t$  with an auto-encoder, quantization and entropy coding. Then, the MC module utilizes the reconstructed MV,  $\hat{v}_t = \bar{v}_t + \hat{d}_t$ , to align the reconstructed frame  $\hat{x}_{t-1}$  to  $x_t$ . The warped frame  $x'_{t-1}$  is enhanced by the DPEG network to generate a compensated frame  $\tilde{x}_t^m$ . After that, the RC module compresses and reconstructs the texture residual  $r_t = x_t - \tilde{x}_t^m$ . Finally, the PQE module receives the residual compensation  $\tilde{x}_t^r = \tilde{x}_t^m + \hat{r}_t$  and the aligned reference  $\tilde{x}_{t-1}'$ , and employs two DPEGs with weighted fusion to obtain the reconstructed frame  $\hat{x}_t$ . Aimed at an optimal RD efficiency, the compression and enhancement processes are jointly trained.

ciency, respectively. [2] designed a scale-space flow to improve the ME robustness under common failure cases, *e.g.*, disocclusion and fast motion. [17] designed a resolution-adaptive flow coding (RaFC) to effectively compress the optical flow maps globally and locally. In [20], the encoder complexity is optimized with less model parameters. In [32], an efficient, learned and flexible video coding (ELFVC) was proposed to support flexible rate coding with high RD efficiency. Recently, [18] and [24] came up with different ways (CNN or GAN) to compress video contents via low-dimensional feature representations, which were further utilized to reconstruct video frames. In our work, the dual-path DPEG network is introduced to extensively reduce the spatial-temporal redundancies of video frames. Compared with the state-of-the-arts, our method shows a significantly increased compression efficiency.

**Visual enhancement.** The visual enhancement techniques are utilized to improve the visual quality of images or videos. Generally, the image enhancement can be achieved by GAN [11, 30] or CNN [22, 36]. In [45], a multi-frame quality enhancement (MFQE) method utilized high-quality frames to enhance low-quality frames, where the high-quality frames were detected with support vector machine (SVM). In [13], the MFQE2.0 method replaced the SVM by bi-directional long short-term memory (BiLSTM) and also improved the convolutional network of MFQE. [41] proposed a task-oriented flow (TOFlow) that demonstrated its superiority to optical flow in video enhancement. [15] leveraged the spatial-temporal relationship of videos and proposed to simultaneously increasing the spatial resolution

and frame rate. Recently, the visual enhancement is also introduced in deep video coding. The HLVC method introduced a separate quality enhancement module at decoder-end [43]. In our work, we incorporate the enhancement module into the reconstruction process, thereby leading to a joint training of video compression and enhancement.

### 3. Proposed Method

**Notations.** Let  $x_t$  denote the  $t$ -th frame of an original video and  $\hat{x}_t$  denote its constructed frame.  $\tilde{x}_t^m$  and  $\tilde{x}_t^r$  represent the compensated frames of  $x_t$  with motion and residual information, respectively. The reconstructed  $(t-1)$ -th frame,  $\hat{x}_{t-1}$ , is sent back for recurrent prediction. It is also aligned to  $x_t$  and  $\tilde{x}_t^r$ , resulting to  $x'_{t-1}$  and  $\tilde{x}_{t-1}'$ , for MC and quality enhancement. The MV matrix of  $x_t$  is predicted as  $\bar{v}_t$  and finally denoted as  $v_t$  after ME. Their difference,  $d_t$ , is compressed and reconstructed as  $\hat{d}_t$ . The difference between  $x_t$  and  $\tilde{x}_t^m$  is represented as a residual  $r_t$ , whose corresponding reconstruction is denoted by  $\hat{r}_t$ .

#### 3.1. The DGVC framework

As shown in Figure 2, the encoder of DGVC consists of 6 modules: ME, MVP, MVDC, MC, RC and PQE. All modules are designed with deep neural networks and jointly trained aimed at an optimized RD performance. This coding procedure applies to all P frames while the context-adaptive entropy model of [21] is utilized to compress I frames.

**ME module.** In DGVC, we employ a bi-directional IPPP structure [44] with a GOP size of 15. The frames 0, 15 are coded as I frames while the others are coded as

P frames. As shown in Figure 3, the frames 1~7 are forwardly predicted from frame 0 while the frames 8~14 are backwardly predicted from frame 15 of next GOP. To remove the temporal redundancies of P frames, the ME module estimates the MV  $v_t$  between adjacent frames:  $x_t$  and  $\hat{x}_{t-1}$ . In this paper, we employ a low-complexity optical flow model, SPyNet [31], which combines spatial pyramid and deep convolutional network for fast ME.

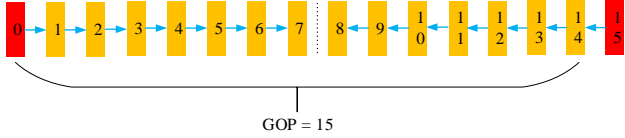


Figure 3. The bi-directional IPPP structure with GOP size 15. Frames 0 and 15 are I frames. Frames 1~7 and 8~14 are forwardly and backwardly predicted P frames, respectively.

**MVP module.** Due to the high spatial-temporal correlation between MVs, it is sensible to compress the MV difference  $d_t$  instead of MV values. We set  $d_t = v_t - \bar{v}_t$ , where  $\bar{v}_t$  is a predicted MV from an MV buffer, which is constituted by the MV information of its three preceding frames. The prediction is achieved by a light network with a convolutional layer, two residual blocks and another two convolutional layers. The channel number is 2 for the last layer and 64 for the others. The convolutional kernel size and stride are  $3 \times 3$  and 1, respectively. Relu is utilized as the activation function in all convolutional layers.

**MVDC module.** The MV difference  $d_t \in R^{H \times W \times 2}$ , where  $H$  and  $W$  are frame height and width, is compressed by MVDC module. To reduce the coding bits, we employ an auto-encoder with four downsampling layers and four upsampling layers that are implemented with convolutions and deconvolutions, respectively. The compact representation  $d_t^c \in R^{\frac{H \times W}{16} \times 128}$  is further processed by quantization and entropy coding, with the procedure presented in [26]. The reconstructed MV can be calculated as  $\hat{v}_t = \bar{v}_t + \hat{d}_t$ .

**MC module.** The MC module utilizes the reconstructed previous frame,  $\hat{x}_{t-1}$  and the reconstructed MV,  $\hat{v}_t$ , to generate a warped frame that is aligned to the current frame  $x_t$ . The warped frame, namely  $x'_{t-1}$ , is fed into the DPEG network to reconstruct an enhanced frame  $\tilde{x}_t^m$ . A ConvLSTM model is deployed to use multiple reference frames in history. This module will be elaborated in Section 3.2.

**RC module.** The motion compensated and enhanced frame  $\tilde{x}_t^m$  is further utilized to calculate the texture residual  $r_t = x_t - \tilde{x}_t^m$ . Its compression is finished with the same process to that of MDVC. After this step, the reconstructed texture residual and compensated frame are represented by  $\hat{r}_t$  and  $\tilde{x}_t^r = \tilde{x}_t^m + \hat{r}_t$ , respectively.

**PQE module.** The last module employs two DPEGs to enhance  $\tilde{x}_t^r$  and  $\tilde{x}'_{t-1}$ , and further combines them as the

constructed frame  $\hat{x}_t$ . In particular,  $\tilde{x}'_{t-1}$  is a warped frame that aligns  $\hat{x}_{t-1}$  to  $\tilde{x}_t^m$ , where the alignment process is realized by an ME and a warping operation. Details of this module will be presented in Section 3.3.

**The decoder.** The compressed stream consists of the compressed MV residual, the compressed texture residual and the previously coded frames, from which we can easily decode  $\hat{d}_t$ ,  $\hat{r}_t$ ,  $\hat{x}_{t-1}$  and  $\bar{v}_t$ . The  $\tilde{x}_t^m$  can be derived with  $\hat{v}_t = \bar{v}_t + \hat{d}_t$ ,  $\hat{x}_{t-1}$  and the MC module. Finally, the reconstructed frame  $\hat{x}_t$  is obtained by  $\tilde{x}_t^r = \tilde{x}_t^m + \hat{r}_t$ ,  $\hat{x}_{t-1}$  and the PQE module.

### 3.2. MC with DPEG network

In video coding, the P frames generally have lower residuals than I frames. The residual at  $t$ -th frame,  $r_t$  is calculated between the current frame  $x_t$  and its previous frame with motion compensation,  $\tilde{x}_t^m$ , where the latter can be obtained by a combination of  $\hat{x}_{t-1}$  and  $\hat{v}_t$ . To further reduce the bits for  $r_t$  under the same visual quality, we employ a two-step method. In the first step, we compensate the previous frame with a non-linear warp,

$$x'_{t-1} = \text{Warp}(\hat{x}_{t-1}, \hat{v}_t); \quad (1)$$

while in the second step, the warped frame is enhanced by our DPEG network,

$$\tilde{x}_t^m = \text{DPEG}(x'_{t-1}). \quad (2)$$

The DPEG network is implemented with GAN and RABs. Recently, the GAN model has achieved significant successes in image enhancement and inpainting, which inspires us to introduce GAN into deep video coding. However, the conventional generator involves a de facto downsampling process to increase its receptive field, whilst excluding the texture details of original frame. This is unhelpful in frame reconstruction that is evaluated by full-reference quality metrics. To address this issue, we add another parallel path with RABs for video details, as shown in Figure 4. To avoid high computational complexity, the DPEG is designed as a compact framework with input  $I$  and output  $I_E$ . In the second step of MC as (2),  $I = x'_{t-1}$ ,  $I_E = \tilde{x}_t^m$ .

**$\alpha$ -path.** To increase the receptive field of low-dimensional features, an encoder is employed with a convolutional layer with stride 1, three convolutional layers with stride 2 and three residual blocks. The obtained semantic features,  $F_{t,1} \in R^{H \times W \times C}$ ,  $F_{t,2} \in R^{\frac{H}{2} \times \frac{W}{2} \times C}$ ,  $F_{t,3} \in R^{\frac{H}{4} \times \frac{W}{4} \times 2C}$ , are fed into  $\beta$ -path and the decoder. After that, a ConvLSTM is inserted to fully utilize the reference information of coded frames. The state and output vectors of ConvLSTM,  $C_{t-1}$  and  $H_{t-1}$ , are fed into current network. The decoder part is set as an inverse process of encoder with upsampling. To avoid semantic information loss,



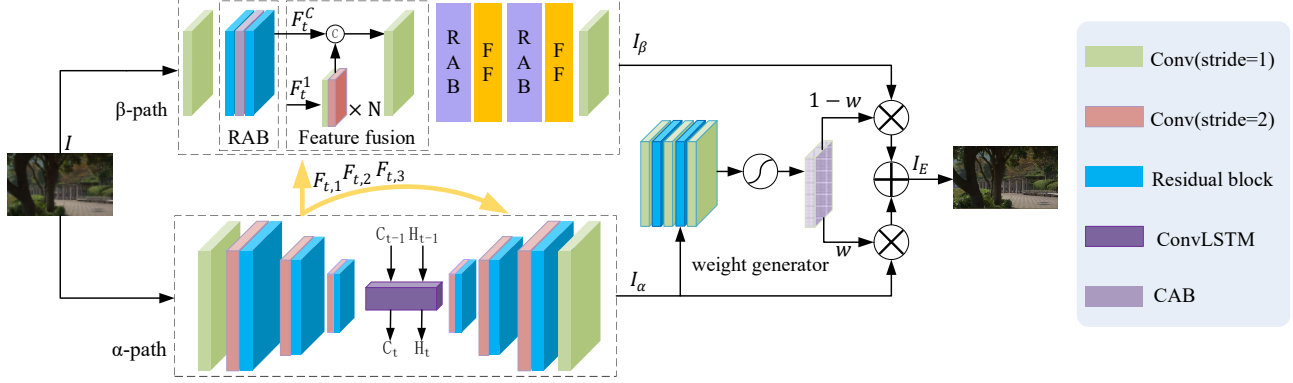


Figure 4. The proposed DPEG for MC and PQE. The  $\alpha$ -path with generator and ConvLSTM focuses on larger receptive field and global structures. The  $\beta$ -path with RABs focuses on smaller receptive field and local textures. The semantic features ( $F_{t,1}, F_{t,2}, F_{t,3}$ ) are fed from  $\alpha$ -path into  $\beta$ -path as a guidance. Finally, a weighted fusion is employed to combine the results of the two paths. The input  $I$  and output  $I_E$  are task-dependent, e.g.  $I = x_{t-1}, I_E = \tilde{x}_t^m$  in MC.

a U-Net [34] is used to skip connect the semantic features to the decoder so that the enhanced results contain the original semantic information.

**$\beta$ -path.** This path consists of two convolution layers with stride 1, three RABs and three feature fusion blocks where downsampling is not applied. An RAB is composed of two residual blocks and a channel attention block (CAB) [46]. Each RAB extracts a feature representation  $F_t^C \in R^{H \times W \times C}$  of  $C$  channels, which is further fused with the semantic feature  $F_{t,k}, k = 1, 2, 3$  from  $\alpha$ -path. The feature fusion block also includes an upsampling process to match the dimensions of features. With a smaller receptive field, there is less access to global features in  $\beta$ -path. Therefore, the fusion of semantic features from  $\alpha$ -path benefits the frame reconstruction.

**Weighted fusion.** To take advantage of both paths, we employ a weighted summation of results:

$$I_E = w \cdot I_\alpha + (1 - w) \cdot I_\beta, \quad (3)$$

where  $w$  is a weight matrix to represent the dependence degree of  $I_E$  on  $I_\alpha$ . We utilize three convolutional layers and two residual blocks to extract the saliency of frame and further warp it to  $(0, 1)$  with a Sigmoid function.

**The discriminator.** The two paths of DPEG are co-trained by the generative-adversarial process after weighted fusion. The discriminator utilizes four downsampling layers aimed at a larger receptive field. Then, it employs the attention mechanism and different pooling strategies to generate two attention maps,  $M_{avg}$  and  $M_{max}$ , and multiplies them with the downsampled frame. Finally, it concatenates the obtained frames and judges them after convolutions. The  $M_{avg}$  and  $M_{max}$  are also important in the loss function for training.

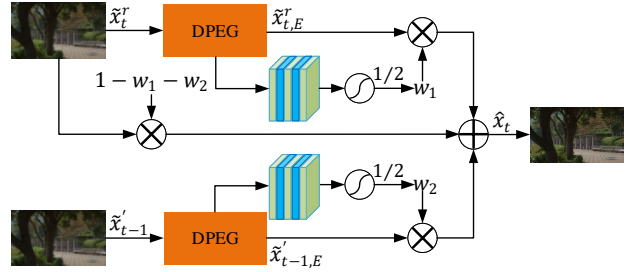


Figure 5. The PQE module with DPEG networks. The constructed frame  $\hat{x}_t$  is composed of three parts: the enhanced result of  $\tilde{x}_t^r$  with weight  $w_1$ , the enhanced result of  $\tilde{x}_{t-1}^r$  with weight  $w_2$  and the  $\tilde{x}_t^r$  with weight  $1 - w_1 - w_2$ .

### 3.3. PQE with DPEG networks

The compensated video frames can be further enhanced before reconstruction. There have been extensively studies to enhance the visual quality or remove compression artifacts of video sequences. The quality enhancement module has also been introduced to decoder-end of deep video compression by [43]. In this paper, we deploy a PQE module before reconstruction, which is jointly trained by the encoder. The DPEG network is reused to construct PQE due to its effectiveness in visual enhancement.

As shown in Figure 5, we employ two DPEG networks to enhance the compensated frame  $\tilde{x}_t^r$  and the aligned previous frame  $\tilde{x}_{t-1}^r$ , respectively. The  $\tilde{x}_t^r$  is compensated by  $\tilde{x}_t^m$  and the reconstructed residual  $\hat{r}_t$ . The  $\tilde{x}_{t-1}^r$  represents the results of aligning  $\hat{x}_{t-1}$  to  $\tilde{x}_t^r$ , where the alignment process is a combination of ME and warping: an MV is firstly calculated by SPyNet and then utilized to warp  $\hat{x}_{t-1}$ :

$$\tilde{x}_{t-1}^r = \text{Warp}(\hat{x}_{t-1}, \text{ME}(\hat{x}_{t-1}, \tilde{x}_t^r)). \quad (4)$$

The  $\tilde{x}_t^r$  and  $\tilde{x}_{t-1}^r$  frames are separately enhanced as  $\tilde{x}_{t,E}^r$  and  $\tilde{x}_{t-1,E}^r$ , which are fused to obtain the final reconstruction  $\hat{x}_t$ :

$$\hat{x}_t = w_1 \cdot \tilde{x}_{t,E}^r + w_2 \cdot \tilde{x}_{t-1,E}^r + (1 - w_1 - w_2) \cdot \tilde{x}_t^r, \quad (5)$$

where the weights  $w_1$  and  $w_2$  are generated with the weight generator in Section 3.2 but are halved to avoid data overflow after summation. The weight  $1 - w_1 - w_2$  is a penalty coefficient in case of enhancement failure.

### 3.4. Joint training of DGVC

Compared with reigning video codecs, the deep video codec has an advantage that its end-to-end framework can be jointly optimized with training on a large-scale dataset. In this paper, we make the first attempt to jointly train the compression and enhancement of deep video coding, aimed at an optimal resource allocation between compressed bitrate and reconstructed visual quality. Our training process consists of two phases. In the first phase (0~300K iterations), we perform a coarse-grain training with the reference frame  $x_{t-1}$  and learning rate  $1e-4$ ; while in the second phase (300K~900K iterations), we perform a fine-grain training with the reference frame  $\hat{x}_{t-1}$  and learning rate  $1e-5$ . In each phase, we successively train the MVP, MVDC, MC, RC, PQE modules and then perform a joint training of all modules. The ME module is performed with the SPyNet without further training.

During training, we employ the following loss functions for the MVP, MVDC, MC, RC, PQE and joint training:

$$\left\{ \begin{array}{l} \mathcal{L}_{MVP} = \text{MSE}(v_t, \bar{v}_t) \\ \mathcal{L}_{MVDC} = \lambda \text{MSE}(d_t, \hat{d}_t) + R_{mvd} \\ \mathcal{L}_{MC} = \mathcal{L}_G \\ \mathcal{L}_{RC} = \lambda \text{MSE}(r_t, \hat{r}_t) + R_{res} \\ \mathcal{L}_{PQE} = D(x_t, \hat{x}_t) \\ \mathcal{L}_{ALL} = \lambda D(x_t, \hat{x}_t) + R_{mvd} + R_{res} \end{array} \right., \quad (6)$$

where MSE denotes the mean squared error.  $R_{mvd}$  and  $R_{res}$  represent the bits consumed by MV difference and residuals after compression, respectively.  $D(\cdot)$  represents the frame-level distortion, which is calculated as MSE and  $1 - \text{MS-SSIM}$  in PSNR-oriented and MS-SSIM-oriented codecs, respectively.  $\lambda$  is a coefficient for RD tradeoff.  $\mathcal{L}_G$  is the loss function for generator of DPEG. The loss functions for generator and discriminator are set as:

$$\begin{aligned} \mathcal{L}_G = & \gamma E_{x \sim \hat{x}} [(x_t - \mathcal{G}(x'_{t-1}))^2] \\ & + E_{x \sim \hat{x}} [1 - \mathcal{D}(\mathcal{G}(x'_{t-1}))^2] \\ & + E_{x \sim \hat{x}} [1 - \phi(\mathcal{G}(x'_{t-1}))^2], \end{aligned} \quad (7)$$

$$\mathcal{L}_D = E_{x \sim \hat{x}} [1 - \mathcal{D}(x_t)^2] + E_{x \sim \hat{x}} [\mathcal{D}(\mathcal{G}(x'_{t-1}))^2], \quad (8)$$

where  $\phi(\cdot)$  represents the calculation of attention maps  $M_{avg}$  and  $M_{max}$ .

## 4. Experiments

### 4.1. Experimental setup

**Datasets.** We train our DGVC with the popular Vimeo-90k [41] dataset, which consists of 89,000 video clips at a resolution of  $448 \times 256$ . To report the performance of our method, we test on H.265 CTC (including Class B at  $1920 \times 1080$ , Class C at  $832 \times 480$  and Class D at  $416 \times 240$ ) [5], MCL-JCV (at  $1920 \times 1080$ ) [40], UVG (at  $1920 \times 1080$ ) [29] and VTL (at  $352 \times 288$ ) [1]. In total, there are 42 HD videos and 23 low-resolution videos are tested.

**Evaluation.** We compare our method with the popular deep codecs FVC [18], Liu’s [24], RLVC [44], Agustsson’s [2], HLVC [43], M-LVC [23], Hu’s [17], Lu’s [25], DVC [26] as well as H.265 implemented by x265 LDP very fast mode. For fair comparison, the results of compared methods are collected from their reports. The consumed bits and reconstruction quality are evaluated by bpp and PSNR/MS-SSIM, respectively. We also calculate the BDBR values [4] that represents the average bit reduction with the same PSNR or MS-SSIM.

**Implementation details.** We implement our model on Tensorflow with all training and testing performed on an NVIDIA RTX 2080Ti GPU. The batch size and  $\gamma$  are set as 4 and 1000, respectively. For PSNR-oriented compression, we train four models with different  $\lambda$  values from 512 to 2560; while for MS-SSIM-oriented compression, we train another four models with  $\lambda$  from 8 to 48. Detailed training process can be seen in Section 3.4.

### 4.2. Experimental results

Figure 6 show the comparison between our DGVC and the state-of-the-arts. To evaluate our method to the maximum extent, we test 6 video groups from 4 datasets and collect all available results of compared codecs. The performances of codecs are shown by two types of curves: PSNR vs. bpp and MS-SSIM vs. bpp. A curve above others is considered with a superior RD performance. **First**, all deep codecs have achieved competitive or superior performances compared with H.265 (x265 LDP very fast), which demonstrates the effectiveness of learning-based video coding. **Second**, the RD performance of deep video coding has been greatly improved since 2019, which demonstrates the potential of learning-based video coding. The recent deep codecs, such as FVC and Liu’s, have significantly surpassed the H.265. We can envision a deep video codec with comparable performance to H.266/VVC in the foreseeable future. **Third**, our DGVC has achieved significantly superior performances than the state-of-the-arts in most datasets. For example, in Class D by PSNR, UVG by MS-SSIM and VTL by PSNR, the DGVC achieve remarkably higher performance even compared with the 2nd best curves. In Class C by PSNR and MS-SSIM, the DGVC achieve comparable

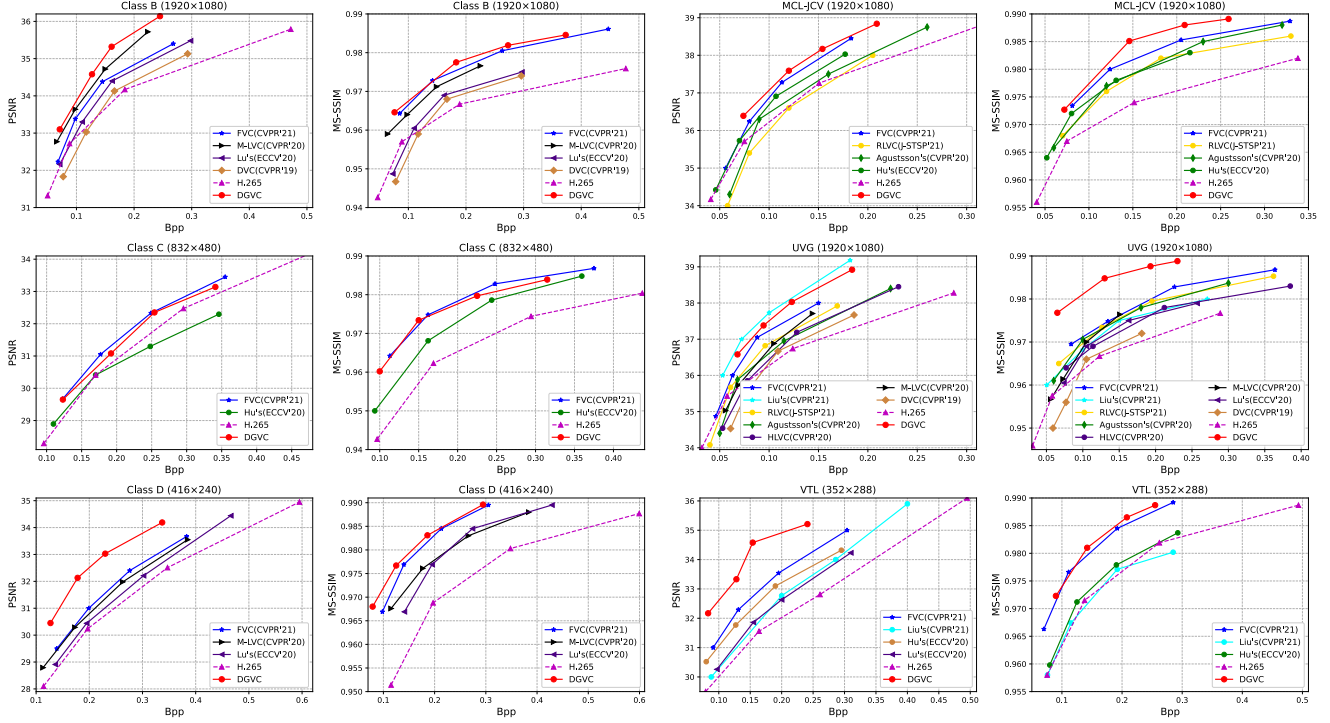


Figure 6. Compression of our DGVC with 9 popular deep codecs and H.265 (x265 LDP very fast). The horizontal and vertical axes represent the coding bit (in bpp) and reconstructed quality (in PSNR or MS-SSIM), respectively. The proposed DGVC exhibits significantly superior or at least competitive performance compared with the state-of-the-arts in each dataset.

Datasets	DVC [26]	Hu's [17]	Lu's [25]	Agustsson's [2]	HLVC [43]	M-LVC [23]	RLVC [44]	Liu's [24]	FVC [18]	DGVC
Class B	5.66/-2.74	-/-	-13.35/-7.93	-/-	-11.75/-37.44	<b>-36.55/-42.82</b>	-24.20/-50.42	-/-	-23.75/ <b>-54.51</b>	<b>-44.19 /-58.29</b>
Class C	25.88/-6.88	4.94/-32.44	-/-	-/-	7.83/-23.63	-/-	-4.67/-35.94	-/-	<b>-14.18 / -43.58</b>	<b>-8.58 /44.10</b>
Class D	15.34/-18.51	-/-32.43	-6.86/-	-/-	-12.57/ <b>-52.56</b>	-13.87/-36.27	<b>-27.01 /48.85</b>	-/-	-18.39/-51.19	<b>-44.72 /-56.38</b>
MCL-JCV	-/-	-10.60/-34.10	4.21/-	-1.82/-33.61	-/-	-/-	-/-	-/-	<b>-22.48 /-52.00</b>	<b>-31.21 / -51.17</b>
UVG	10.40/8.05	-/-	-7.56/-25.49	-8.80/-38.04	-1.37/-30.12	-12.11/-25.44	-13.48/-40.62	<b>-49.42 /-30.70</b>	-28.71/ <b>-45.25</b>	<b>-47.62 / -77.60</b>
VTL	-/-	-/-6.04	-16.05/-	-/-	-/-	-/-	-/-	-9.51/2.42	<b>-28.10 / -39.44</b>	<b>-60.02 /-41.98</b>
Average	<b>8.03/-5.02</b>	<b>-2.83/-26.25</b>	<b>-7.92/-16.71</b>	<b>-5.31/-35.83</b>	<b>-4.47/-35.94</b>	<b>-20.84/-34.84</b>	<b>-17.34/-43.96</b>	<b>-29.4 /-14.14</b>	<b>-22.60/ -46.66</b>	<b>-39.39 /-54.92</b>

Table 1. Compression on BDBR results calculated by the PSNR vs. bpp and MS-SSIM vs. bpp curves. H.265 is set as the benchmark. In all cases, our DGVC achieves the best or 2nd best BDBR performance. On average, it significantly outperforms the state-of-the-arts.

performances to FVC. While in other figures, the DGVC also surpasses all compared methods. These facts undoubtedly demonstrates the superiority of our DGVC model.

To quantitatively compare the video codecs, we also present the BDBR results (with PSNR and MS-SSIM) of all available curves in Table 1. H.265 is set as the benchmark to calculate all values. The results in table are consistent with those in Figure 6 that our DGVC always ranks the best or 2nd best in all datasets. An interesting result occurs when comparing FVC with DGVC in MCL-JCV by MS-SSIM. The RD curves indicates DGVC is superior while the BDBR slightly prefers the FVC. This conflict is due to the different definition domains to interpolate and calculate BDBR [4]. On average, the DGVC achieves a BDBR of -39.39% or -54.92% by PSNR or MS-SSIM, which also sup-

ports the superior efficiency of the DGVC.

### 4.3. Ablation study

**Contributions of individual modules.** In DGVC, we design an MVP with a light network, an MC with DPEG network, a PQE with DPEG networks and a joint training, as shown in Figure 2. To examine the contributions of these modules, we perform the following ablation study. A baseline method with a simple but feasible framework (ME+MVDC+MC w/o DPEG+RC) is examined first. Then, our designed modules (MVP, MC w/ DPEG, PQE, joint training) are introduced sequentially to observe their RD improvements. The average results on CTC class D are summarized in Figure 7. With more designed modules, the RD performance is continuously improved. For example,

with PSNR=32dB, the bpps of the five settings are 0.47, 0.45, 0.28, 0.20, 0.17, respectively, which indicate the bpp savings at 4.3%, 37.8%, 28.6% and 15.0% by introducing MVP, MC w/ DPEG, PQE and joint training. This fact reveals the effectiveness of our design, especially for the DPEG-based MC/PQE and the joint training.

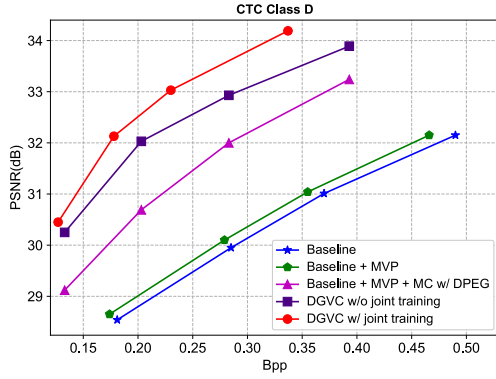


Figure 7. Contributions of individual modules. The following settings are compared: (i) Baseline (ME+MVDC+MC w/o DPEG+RC); (ii) Baseline + MVP; (iii) Baseline + MVP + MC w/ DPEG; (iv) DGVC w/o joint training (Baseline + MVP + MC w/ DPEG + PQE); (v) DGVC w/ joint training. The RD performances are kept improved with more modules, which demonstrates the effectiveness of our design.

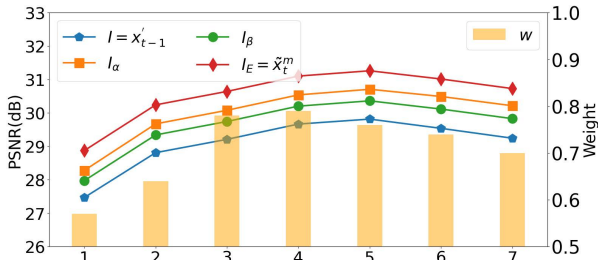


Figure 8. Comparison between the input ( $I$ ), the intermediate results ( $I_\alpha$ ,  $I_\beta$ ) and the output ( $I_E$ ) of DPEG in MC. The results are obtained by averaging the 1~7-th frames of all Class D sequences.  $w$  indicates the weight for fusion. Each path has its own contributions to the final output.

**Contributions of individual paths in DPEG.** In Figure 4, we set an  $\alpha$ -path with auto-encoder and ConvLSTM and a  $\beta$ -path with RABs. We fuse the outputs of both paths to generate the result. In Figure 8, we compare the input ( $I = x_{t-1}$ ), the intermediate results ( $I_\alpha$ ,  $I_\beta$ ) and the output ( $I_E = \tilde{x}_t^m$ ) of DPEG in MC. It can be seen that both  $I_\alpha$  and  $I_\beta$  improve the PSNR of  $I$ , which indicates the effectiveness of both paths. By fusing the results of  $I_\alpha$  and  $I_\beta$  with  $w$  ( $w > 0.5$  when  $I_\alpha$  has a better visual quality), the resulted  $I_E$  achieve a further high performance, which implies the

complementarity between the  $\alpha$ -path and  $\beta$ -path as well as the effectiveness of our weight fusion.

**Contributions of DPEG networks in PQE.** Figure 5 utilizes two DPEG networks to enhance  $\tilde{x}_t^r$  and  $\tilde{x}_{t-1}^r$  as  $\tilde{x}_{t,E}^r$  and  $\tilde{x}_{t-1,E}^r$ , respectively. Then, it applies a weighted sum of  $\tilde{x}_t^r$ ,  $\tilde{x}_{t,E}^r$  and  $\tilde{x}_{t-1,E}^r$  to obtain the final reconstruction  $\hat{x}_t$ . Figure 9 shows the average PSNR values of these pictures. Obviously, each DPEG network contributes to the final performance. With a weighted fusion of all enhanced pictures, the finally reconstructed frame  $\hat{x}_t$  is of a high visual quality in terms of PSNR. Therefore, it is reasonable to apply two DPEG networks in the PQE module of DGVC.

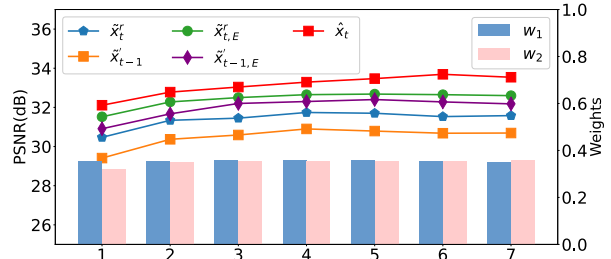


Figure 9. Comparison between the inputs ( $\tilde{x}_t^r$ ,  $\tilde{x}_{t-1}^r$ ), the intermediate results ( $\tilde{x}_{t,E}^r$ ,  $\tilde{x}_{t-1,E}^r$ ) and the output ( $\hat{x}_t$ ) of PQE with DPEG. The results are obtained by averaging the 1~7-th frames of all Class D sequences.  $w_1$ ,  $w_2$  indicate the weights for fusion. After DPEG, both input frames are enhanced and further fused to generate the reconstructed frame  $\hat{x}_t$  that is of the highest quality among all these results.

#### 4.4. Limitations

Nowadays, the H.266/VVC incorporates the enhanced block partitioning, diversified intra and inter predictions, refined ME and MC, extended transform and quantization, improved entropy coding and adaptive deblocking filters with RD optimization (RDO) [6]. As a contrast, the deep video codecs, including our DGVC and all compared methods [2, 17, 18, 23–26, 43, 44], are still imitating the traditional coding modules, which limits their RD performances compared with the newest video coding standard. In such sense, the development of more deep coding methods are imperative to realize more advanced video coding techniques. A hybrid framework to take advantages of all deep codecs is feasible. In addition, the deep video codecs prevail in the utilization of big video data. With a joint training of all modules on large-scale datasets, the deep video coding has a brighter outlook in a foreseeable future.

#### 5. Conclusions

Nowadays, the deep video codecs have been extensively studied with ever-increasing RD performance. In this paper,



we proposed an end-to-end deep video codec called DGVC that consists of ME, MVP, MVDC, MC, RC and PQE modules. We designed a DPEG network with dual-path enhancement and fusion, whose efficiency was demonstrated in experimental results. We reused the DPEG network in both MC and PQE modules and also employed a joint training of deep video compression and enhancement. Comprehensive studies on four popular datasets have demonstrated the RD efficiency of our DGVC method, which outperformed the state-of-the-art deep video codecs.

## References

- [1] Video trace library. <http://trace.eas.asu.edu/yuv/index.html>. 2001. 6
- [2] Eirikur Agustsson, David Minnen, Nick Johnston, Johannes Ballé, Sung Jin Hwang, and George Toderici. Scale-space flow for end-to-end optimized video compression. In *2020 IEEE/CVF Conference on Computer Vision and Pattern Recognition (CVPR)*, pages 8500–8509, 2020. 2, 3, 6, 7, 8
- [3] Fabrice Bellard. BPG image format. <https://bellard.org/bpg/>. 2
- [4] Gisle Bjontegaard. Calculation of average psnr differences between rd-curves. *Doc. VCEG-M33, ITU-T Video Coding Experts Group (VCEG)*, Jan. 2001. 6, 7
- [5] Frank Bossen. Common test conditions and software reference configurations. *Doc. JCTVC-L1100, Joint Collaborative Team on Video Coding (JCT-VC)*, Jan. 2013. 6
- [6] Benjamin Bross, Ye-Kui Wang, Yan Ye, Shan Liu, Jianle Chen, Gary J. Sullivan, and Jens-Rainer Ohm. Overview of the versatile video coding (vvc) standard and its applications. *IEEE Transactions on Circuits and Systems for Video Technology*, 31(10):3736–3764, 2021. 1, 8
- [7] Chunlei Cai, Li Chen, Xiaoyun Zhang, and Zhiyong Gao. End-to-end optimized ROI image compression. *IEEE Transactions on Image Processing*, 29:3442–3457, 2020. 1, 2
- [8] Jianrui Cai, Zisheng Cao, and Lei Zhang. Learning a single tucker decomposition network for lossy image compression with multiple bits-per-pixel rates. *IEEE Transactions on Image Processing*, 29:3612–3625, 2020. 1, 2
- [9] Li-Heng Chen, Christos G. Bampis, Zhi Li, Andrey Norkin, and Alan C. Bovik. ProxIQ: A proxy approach to perceptual optimization of learned image compression. *IEEE Transactions on Image Processing*, 30:360–373, 2021. 1, 2
- [10] Tong Chen, Haojie Liu, Zhan Ma, Qiu Shen, Xun Cao, and Yao Wang. End-to-end learnt image compression via non-local attention optimization and improved context modeling. *IEEE Transactions on Image Processing*, 30:3179–3191, 2021. 1, 2
- [11] Yu-Sheng Chen, Yu-Ching Wang, Man-Hsin Kao, and Yung-Yu Chuang. Deep Photo Enhancer: Unpaired learning for image enhancement from photographs with GANs. In *2018 IEEE/CVF Conference on Computer Vision and Pattern Recognition (CVPR)*, pages 6306–6314, 2018. 3
- [12] Zhengxue Cheng, Heming Sun, Masaru Takeuchi, and Jiro Katto. Learned image compression with discretized gaussian mixture likelihoods and attention modules. In *2020 IEEE/CVF Conference on Computer Vision and Pattern Recognition (CVPR)*, pages 7936–7945, 2020. 1, 2
- [13] Zhenyu Guan, Qunliang Xing, Mai Xu, Ren Yang, Tie Liu, and Zulin Wang. MFQE 2.0: A new approach for multi-frame quality enhancement on compressed video. *IEEE Transactions on Pattern Analysis and Machine Intelligence*, 43(3):949–963, 2021. 3
- [14] Amirhossein Habibi, Ties Van Rozendaal, Jakub Tomczak, and Taco Cohen. Video compression with rate-distortion autoencoders. In *2019 IEEE/CVF International Conference on Computer Vision (ICCV)*, pages 7032–7041, 2019. 2
- [15] Muhammad Haris, Greg Shakhnarovich, and Norimichi Ukita. Space-time-aware multi-resolution video enhancement. In *2020 IEEE/CVF Conference on Computer Vision and Pattern Recognition (CVPR)*, pages 2856–2865, 2020. 3
- [16] Dailan He, Yaoyan Zheng, Baocheng Sun, Yan Wang, and Hongwei Qin. Checkerboard context model for efficient learned image compression. In *2021 IEEE/CVF Conference on Computer Vision and Pattern Recognition (CVPR)*, pages 14766–14775, 2021. 1, 2
- [17] Zhihao Hu, Zhenghao Chen, Dong Xu, Guo Lu, Wanli Ouyang, and Shuhang Gu. Improving deep video compression by resolution-adaptive flow coding. In *Proceedings of the European Conference on Computer Vision (ECCV)*, pages 193–209, 2020. 2, 3, 6, 7, 8
- [18] Zhihao Hu, Guo Lu, and Dong Xu. FVC: A new framework towards deep video compression in feature space. In *2021 IEEE/CVF Conference on Computer Vision and Pattern Recognition (CVPR)*, pages 1502–1511, 2021. 2, 3, 6, 7, 8
- [19] Nick Johnston, Damien Vincent, David Minnen, Saurabh Covell, Michele Singh, Troy Chinen, Sung Jin Hwang, Joel Shor, and George Toderici. Improved lossy image compression with priming and spatially adaptive bit rates for recurrent networks. In *2018 IEEE/CVF Conference on Computer Vision and Pattern Recognition (CVPR)*, pages 4385–4393, 2018. 1, 2
- [20] Jan P. Klopp, Keng-Chi Liu, Shao-Yi Chien, and Liang-Gee Chen. Online-trained upsampler for deep low complexity video compression. In *Proceedings of the IEEE/CVF International Conference on Computer Vision (ICCV)*, pages 7929–7938, 2021. 2, 3
- [21] Jooyoung Lee, Seunghyun Cho, and Seung-Kwon Beack. Context-adaptive entropy model for end-to-end optimized image compression. In *Proceedings of the International Conference on Learning Representations (ICLR)*, 2019. 1, 2, 3
- [22] Chongyi Li, Chunle Guo, and Change Loy Chen. Learning to enhance low-light image via zero-reference deep curve estimation. *IEEE Transactions on Pattern Analysis and Machine Intelligence*, pages 1–1, 2021. 3
- [23] Jianping Lin, Dong Liu, Houqiang Li, and Feng Wu. M-LVC: Multiple frames prediction for learned video compression. In *2020 IEEE/CVF Conference on Computer Vision and Pattern Recognition (CVPR)*, pages 3543–3551, 2020. 2, 6, 7, 8

- [24] Bowen Liu, Yu Chen, Shiyu Liu, and Hun-Seok Kim. Deep learning in latent space for video prediction and compression. In *2021 IEEE/CVF Conference on Computer Vision and Pattern Recognition (CVPR)*, pages 701–710, 2021. [2](#), [3](#), [6](#), [7](#), [8](#)
- [25] Guo Lu, Chunlei Cai, Xiaoyun Zhang, Li Chen, Wanli Ouyang, Dong Xu, and Zhiyong Gao. Content adaptive and error propagation aware deep video compression. In *Proceedings of the European Conference on Computer Vision (ECCV)*, pages 456–472, 2020. [2](#), [6](#), [7](#), [8](#)
- [26] Guo Lu, Wanli Ouyang, Dong Xu, Xiaoyun Zhang, Chunlei Cai, and Zhiyong Gao. DVC: An end-to-end deep video compression framework. In *2019 IEEE/CVF Conference on Computer Vision and Pattern Recognition (CVPR)*, pages 10998–11007, 2019. [2](#), [4](#), [6](#), [7](#), [8](#)
- [27] Guo Lu, Xiaoyun Zhang, Wanli Ouyang, Li Chen, Zhiyong Gao, and Dong Xu. An end-to-end learning framework for video compression. *IEEE Transactions on Pattern Analysis and Machine Intelligence*, 43(10):3292–3308, 2021. [2](#)
- [28] Haichuan Ma, Dong Liu, Ning Yan, Houqiang Li, and Feng Wu. End-to-end optimized versatile image compression with wavelet-like transform. *IEEE Transactions on Pattern Analysis and Machine Intelligence*, pages 1–1, 2020. [1](#), [2](#)
- [29] Alexandre Mercat, Marko Viitanen, and Jarno Vanne. UVG dataset: 50/120fps 4K sequences for video codec analysis and development. In *MMSys '20: 11th ACM Multimedia Systems Conference*, 2020. [6](#)
- [30] Zhangkai Ni, Wenhan Yang, Shiqi Wang, Lin Ma, and Sam Kwong. Towards unsupervised deep image enhancement with generative adversarial network. *IEEE Transactions on Image Processing*, 29:9140–9151, 2020. [3](#)
- [31] Anurag Ranjan and Michael J. Black. Optical flow estimation using a spatial pyramid network. In *2017 IEEE Conference on Computer Vision and Pattern Recognition (CVPR)*, pages 2720–2729, 2017. [4](#)
- [32] Oren Rippel, Alexander G. Anderson, Kedar Tatwawadi, Sanjay Nair, Craig Lytle, and Lubomir Bourdev. ELF-VC: Efficient learned flexible-rate video coding. In *Proceedings of the IEEE/CVF International Conference on Computer Vision (ICCV)*, pages 14479–14488, 2021. [2](#), [3](#)
- [33] Oren Rippel, Sanjay Nair, Carissa Lew, Steve Branson, Alexander Anderson, and Lubomir Bourdev. Learned video compression. In *2019 IEEE/CVF International Conference on Computer Vision (ICCV)*, pages 3453–3462, 2019. [2](#)
- [34] Olaf Ronneberger, Philipp Fischer, and Thomas Brox. U-Net: Convolutional networks for biomedical image segmentation. In *2015 Medical Image Computing and Computer-Assisted Intervention (MICCAI)*, pages 234–241, 2015. [5](#)
- [35] Xingjian Shi, Zhourong Chen, Hao Wang, Dit-Yan Yeung, Wai-Kin Wong, and Wang-Chun Woo. Convolutional LSTM Network: A machine learning approach for precipitation nowcasting. In *Proceedings of the 28th International Conference on Neural Information Processing Systems - Volume 1*, page 802–810. MIT Press, 2015. [2](#)
- [36] Taeyoung Son, Juwon Kang, Namyup Kim, Sunghyun Cho, and Suha Kwak. URIE: Universal image enhancement for visual recognition in the wild. In *Proceedings of the European Conference on Computer Vision (ECCV)*, pages 749–765, 2020. [3](#)
- [37] Gary J. Sullivan, Jens-Rainer Ohm, Woo-Jin Han, and Thomas Wiegand. Overview of the high efficiency video coding (HEVC) standard. *IEEE Transactions on Circuits and Systems for Video Technology*, 22(12):1649–1668, 2012. [1](#)
- [38] David.S. Taubman and Michael.W. Marcellin. JPEG2000: standard for interactive imaging. *Proceedings of the IEEE*, 90(8):1336–1357, 2002. [2](#)
- [39] G.K. Wallace. The JPEG still picture compression standard. *IEEE Transactions on Consumer Electronics*, 38(1):xviii–xxxiv, 1992. [2](#)
- [40] Haiqiang Wang, Weihao Gan, Sudeng Hu, Joe Yuchieh Lin, Lina Jin, Longguang Song, Ping Wang, Ioannis Katsavounidis, Anne Aaron, and C.-C. Jay Kuo. Mcl-jcv: A jnd-based h.264/avc video quality assessment dataset. In *2016 IEEE International Conference on Image Processing (ICIP)*, pages 1509–1513, 2016. [6](#)
- [41] Tianfan Xue, Baian Chen, Jiajun Wu, Donglai Wei, and William T. Freeman. Video enhancement with task-oriented flow. *International Journal of Computer Vision*, 127(8):1106–1125, 2019. [3](#), [6](#)
- [42] Fei Yang, Luis Herranz, Yongmei Cheng, and Mikhail G. Mozerov. Slimmable compressive autoencoders for practical neural image compression. In *2021 IEEE/CVF Conference on Computer Vision and Pattern Recognition (CVPR)*, pages 4996–5005, 2021. [1](#), [2](#)
- [43] Ren Yang, Fabian Mentzer, Luc Van Gool, and Radu Timofte. Learning for video compression with hierarchical quality and recurrent enhancement. In *2020 IEEE/CVF Conference on Computer Vision and Pattern Recognition (CVPR)*, pages 6627–6636, 2020. [2](#), [3](#), [5](#), [6](#), [7](#), [8](#)
- [44] Ren Yang, Fabian Mentzer, Luc Van Gool, and Radu Timofte. Learning for video compression with recurrent auto-encoder and recurrent probability model. *IEEE Journal of Selected Topics in Signal Processing*, 15(2):388–401, 2021. [2](#), [3](#), [6](#), [7](#), [8](#)
- [45] Ren Yang, Mai Xu, Zulin Wang, and Tianyi Li. Multi-frame quality enhancement for compressed video. In *2018 IEEE/CVF Conference on Computer Vision and Pattern Recognition (CVPR)*, pages 6664–6673, 2018. [3](#)
- [46] Yulun Zhang, Kunpeng Li, Kai Li, Lichen Wang, Bineng Zhong, and Yun Fu. Image super-resolution using very deep residual channel attention networks. In *Proceedings of the European conference on computer vision (ECCV)*, pages 286–301, 2018. [5](#)